AIAA 03–3830

Calculation of Airfoil Flutter by an Euler Method with Approximate Boundary Conditions

C. Gao, S. Luo, F. Liu
Department of Mechanical and Aerospace Engineering
University of California, Irvine, CA 92697-3975

D. M. Schuster
Aeroelasticity Branch
NASA Langley Research Center, Hampton, VA 23681

16th AIAA Computational Fluid Dynamics Conference
June 23–26, 2003/Orlando, FL

Calculation of Airfoil Flutter by an Euler Method with Approximate Boundary Conditions

C. Gao*, S. Luo†, F. Liu‡
Department of Mechanical and Aerospace Engineering
University of California, Irvine, CA 92697-3975

D. M. Schuster§
Aeroelasticity Branch
NASA Langley Research Center, Hampton, VA 23681

This paper demonstrates an efficient numerical method for solving the unsteady Euler equations coupled with the aeroelastic equations for a moving airfoil mounted on linear and torsional springs on stationary Catersian grids. Wall boundary conditions are implemented on non-moving mean chord positions by assuming the airfoil being thin and undergoing small deformation, whereas the full nonlinear Euler equation is used in the field for accurate resolution of shock waves and vorticity, and the mean angle of attack of the body can be large. The method does not require the generation of moving body-fitted grids and thus can be easily deployed in any fluid-structure interaction problem involving relatively small deformation of a thin body. The first-order wall boundary conditions are used in solving the full Euler equations, and the results are compared with the Euler solutions using the exact boundary conditions and known experimental data. It is shown that the first-order boundary conditions are adequate to represent airfoils of typical thicknesses with small deformation for both steady and unsteady calculations. Flutter boundaries are accurately predicted by this method for the Isogai wing model test case.

I. Nomenclature

b	Airfoil half chord = $c/2$
c	Airfoil chord
C_l	Lift coefficient
C_m	Moment coefficient around quarter chord, positive nose up
C_p	Pressure coefficient
$(\mathbf{e}_x, \mathbf{e}_y)$	Unit vectors in (x, y) directions
E	Total specific energy
$F(t, x)$	Instantaneous upper-surface of airfoil
$G(t, x)$	Instantaneous lower-surface of airfoil
$f(x)$	Mean upper-surface of airfoil
$g(x)$	Mean lower-surface of airfoil
$\mathbf{G}$	Euler flux vector
H	Total specific enthalpy
(i, j)	Grid point index
M_∞	Freestream Mach number
$\mathbf{n}$	Outer normal vector to cell surface
n	Real time level
p	Pressure
$\mathbf{q}$	Velocity vector of fluid particle
$\mathbf{q}_b$	Velocity vector of the surface of control volume
R	Flux residual
R^*	Modified residual
S	Surface of control volume
t	Real time
t^*	Pseudo-time
U_∞	Free stream velocity
u, v	x and y velocity components of fluid particle
u_b, v_b	x and y components of grid velocity
V	Control volume
$\mathbf{W}$	Euler conservative flow variable
x, y	Cartesian coordinates
x_0	x-coordinate of the pivot point of airfoil pitching
α	Instantaneous angle of attack, deg
α_m	Mean angle of attack, deg
α_1	Instantaneous increment of angle of attack, deg
α_0	Amplitude of the pitching oscillation
Δt	Real-time step
γ	Ratio of specific heats
κ	Reduced frequency
μ	mass ratio
ρ	Air density
ω	Angular frequency

*Visiting Associate Researcher. Associate Professor, Northwestern Polytechnical University, Xi'an, China.
†Researcher.
‡Associate Professor. Senior Member AIAA.
§Senior Research Engineer. Associate Fellow AIAA

II. Introduction

Computational Fluid Dynamics (CFD) has proven to be a useful tool for the simulation and prediction of buffet, flutter, and Limit Cycle Oscillation (LCO) phenomena of aeroelastic systems. Methods ranging from the linear doublet-lattice method[1] to methods that solve the Euler and the Navier-Stokes equations have been developed.[2–7] Despite its limit in handling transonic and other nonlinear flows, the linear doublet lattice method has been and is still the workhorse for actual design analysis in industry because of its efficiency in computer time and, perhaps equally important, the ease in setting up the computational problem. The Reynolds-Averaged-Navier-Stokes (RANS) methods encompass the most complete flow model short of Large-Eddy-Simulations (LES) or Direct-Numerical-Simulations (DNS). However, RANS simulations for aeroelasticity problems at present demand computational resources beyond those tolerable in a design environment. In addition, their usefulness is limited by uncertainties in turbulence modeling, grid resolution, and numerical damping effects,[6,7] difficulties in grid generation and the transfer of displacements and aerodynamic forces between the structural and aerodynamic grids, and lack of fast and robust algorithms for deforming grids needed in the unsteady computations. In between the above two extremes, methods based on the various forms of the potential flow equation with boundary-layer corrections have shown good results for flutter simulations without the use of large computational resources and with less human work in setting up the computational problem including grid generation. Among such methods, the CAP-TSD[8–10] code is widely known and used. The CAP-TSD code has many advantages over a full-fledged RANS code. These include 1) ease in generating a grid; 2) no need to do complex interpolation between the structural and CFD grids; 3) no need to have a moving grid; 4) less demand on CPU time and memory.

Despite the use of vortex and entropy corrections, the potential flow assumption in CAP-TSD limits its applicability to irrotational flows with weak shocks. Advances in computer speed and maturity of algorithms for the Euler equations have made the solution of the Euler equations a rather dependable and routine tool. Although the Euler equations cannot account for the viscous effects in the boundary layer, it is capable of resolving strong shocks and transporting vortices correctly. Due to the requirement of large computing resources by a Navier-Stokes code and also unresolved issues regarding accuracy of current numerical algorithms for the Navier-Stokes equations, the Euler equations strike a good balance between completeness of the flow model and computational efficiency. In order to retain the ease in setting up a computational grid as in the CAP-TSD code, this paper develops an efficient unsteady Euler solver for aeroelastic applications on stationary Cartesian grids through the use of approximate boundary conditions. The full Euler boundary conditions on the airfoil surface are replaced by their first-order expansions on the mean chord line of the airfoil for thin airfoils with small deformations, which is usually the case for flutter predictions for moving or deforming airfoils. By using these approximate boundary conditions, we can avoid the use of a body-fitted moving or deforming grid, which can be a rather time-consuming task for practical problems. The basic unsteady Euler solver is based on a a finite-volume code called NS83 using an implicit scheme with dual time-stepping.[11,12] Details of the mathematical formulation of the approximate boundary conditions are presented along with their implementation in the finite-volume code. The authors already demonstrated the effectiveness of this approximate method for steady flow calculations.[13] Here, we extend it to unsteady flows and investigate its use for coupled unsteady fluid-structure simulations for an airfoil. Numerical examples are given and the results are compared with those obtained by other methods with full boundary condtions and experimental data whenever available. Discussions and conclusions are finally drawn.

III. Euler Equations and Time-Accurate Scheme

Consider a moving and possibly deforming control volume (computational cell) V in two dimensions whose boundary S moves at velocity (u_b, v_b). The two-dimensional unsteady Euler equations in conservative integral form in the Cartesian coordinate system (x, y) for such a control volume are

$$\frac{\partial}{\partial t}\int_V \mathbf{W} dV + \int_S \mathbf{G}\cdot\mathbf{n} dS = 0 \tag{1}$$

where

$$\mathbf{W} = \begin{bmatrix} \rho \\ \rho u \\ \rho v \\ \rho E \end{bmatrix} \tag{2}$$

$$\mathbf{G} = \begin{bmatrix} \rho(\mathbf{q}-\mathbf{q}_b) \\ \rho u(\mathbf{q}-\mathbf{q}_b) + p\mathbf{e}_x \\ \rho v(\mathbf{q}-\mathbf{q}_b) + p\mathbf{e}_y \\ \rho E(\mathbf{q}-\mathbf{q}_b) + p(u\mathbf{e}_x + v\mathbf{e}_y) \end{bmatrix} \tag{3}$$

$$\mathbf{q} = u\mathbf{e}_x + v\mathbf{e}_y \tag{4}$$

$$\mathbf{q}_b = u_b\mathbf{e}_x + v_b\mathbf{e}_y \tag{5}$$

$$E = \frac{1}{\gamma - 1}\frac{p}{\rho} + \frac{1}{2}(u^2 + v^2) \tag{6}$$

Applying (1) to each cell in the mesh we obtain a set of ordinary differential equations of the form

$$\frac{d}{dt}(\mathbf{W}_{i,j}V_{i,j}) + \mathbf{R}(\mathbf{W}_{i,j}) = 0 \tag{7}$$

where $V_{i,j}$ is the volume of the i,j cell and the residual $\mathbf{R}(\mathbf{W}_{i,j})$ is obtained by evaluating the flux integral in (1). Following Jameson,[11] we approximate the $\frac{d}{dt}$ operator by an implicit backward difference formula of second-order accuracy in the following form (dropping the subscripts i,j for clarity)

$$\frac{3}{2\Delta t}[\mathbf{W}^{n+1}V^{n+1}] - \frac{2}{\Delta t}[\mathbf{W}^nV^n] + \frac{1}{2\Delta t}[\mathbf{W}^{n-1}V^{n-1}] + \mathbf{R}(\mathbf{W}^{n+1}) = 0 \tag{8}$$

Eqn. (8) can be solved for $\mathbf{W}^{n+1}$ at each time step by solving the following steady-state problem in a pseudo time t^*.

$$\frac{d\mathbf{W}}{dt^*} + \mathbf{R}^*(\mathbf{W}) = 0 \tag{9}$$

where

$$\mathbf{R}^*(\mathbf{W}) = \mathbf{R}(\mathbf{W}) + \frac{3}{2\Delta t}(\mathbf{W}V^{n+1}) - \frac{2}{\Delta t}(\mathbf{W}^nV^n) + \frac{1}{2\Delta t}(\mathbf{W}^{n-1}V^{n-1}) \tag{10}$$

Eqn. (9) is solved by an explicit time-marching scheme in t^* for which the local time stepping, residual smoothing, and multigrid techniques[14] can be used to accelerate convergence to a steady state.

In the present approximate method, the grid does not change with the time even for unsteady flow calculations. Thus, in the above equations the cell volume V satisfies $V^{n+1} = V^n = V^{n-1} = V$, and $\mathbf{q}_b = 0$.

IV. Approximate Boundary Conditions

A thin airfoil slightly moving or deforming about its mean position is considered. The mean position of the airfoil chord lies on the horizontal axis x of the coordinate system between $x = 0$ and $x = 1$. The velocity of the incoming uniform free stream makes an angle α_m with the x axis. In the present paper, the airfoil is assumed to be of rigid shape but performs an oscillating motion around a fixed point on its chord line at $x = x_0$. The shape of the airfoil is described by $y = f(x)$ and $g(x)$ for its upper and lower surfaces, respectively. The instantaneous position of the airfoil is described by $y = F(t,x)$ and $y = G(t,x)$ for the upper and lower surfaces, respectively. The flow is assumed inviscid. The boundary conditions on the upper surface of the airfoil at an instant t is

$$v(t,x,F) = u(t,x,F)F_x + F_t \tag{11}$$

where the subscripts, x and t denote the partial derivatives with respect to x and t, respectively. Under the assumption, $|F| \ll 1$, the first-order approximation of (11) on the x axis is

$$v(t,x,0) = u(t,x,0)F_x + F_t + O(F) \tag{12}$$

where $O(F)$ represents terms of the same order of magnitude as F or higher.

The boundary condition on the lower surface is treated similarly. The mean position of the leading edge of the airfoil is chosen as the origin of the coordinate system. If the leading edge is blunt, the boundary condition there is replaced by

$$u = 0 \tag{13}$$

At the sharp trailing edge of the airfoil, the pressures on the upper and lower surfaces should be equal to each other. In supercritical flow with adiabatic shock waves, the velocities and densities at the sharp trailing edge on the upper and lower surfaces may not be equal to each other. It is known that the Kutta condition at the sharp trailing edge is satisfied automatically in Euler calculations.

There are altogether four independent variables in the Euler equations (1), e.g. ρ, u, v and p. In addition to the boundary conditions of the velocity given above, more conditions are needed on the airfoil surfaces. The momentum differential equation in the outward normal direction $\mathbf{n}$ is also used, which gives

$$\mathbf{n}\cdot[\frac{\partial\mathbf{q}}{\partial t} + (\mathbf{q}\cdot\nabla)\mathbf{q}] = \mathbf{n}\cdot(-\frac{\nabla p}{\rho}) \tag{14}$$

On the upper surface of the airfoil, $y = F(t,x)$, the above equation becomes

$$p_y(t,x,F) = F_xp_x(t,x,F) - \rho(t,x,F)[F_{tt} + 2F_{tx}u(t,x,F) + F_{xx}u^2(t,x,F)] \tag{15}$$

The first-order approximation of the above equation is

$$p_y(t,x,0) = F_xp_x(t,x,0) - \rho(t,x,0)[F_{tt} + 2F_{tx}u(t,x,0) + F_{xx}u^2(t,x,0)] + O(F) \tag{16}$$

The corresponding equations on the lower surface of the airfoil are similarly derived.

In this paper, a rigid airfoil performing pitching oscillation about a point at $x = x_0$ on its mean chord is considered as an example. The instantaneous angle of the pitching rotation from the mean position is $\alpha_1(t)$, positive in clockwise direction. Given $f(x)$, the instantaneous ordinate of the upper surface, $F(t,x)$, is expressed implicitly as follows.

$$F\cos\alpha_1 + (x - x_0)\sin\alpha_1 = f\left(x_0 + (x - x_0)\cos\alpha_1 - F\sin\alpha_1\right) \quad (17)$$

where the expression $x_0 + (x - x_0)\cos\alpha_1 - F\sin\alpha_1$ in the first pair of parentheses on the right-hand-side of the equation is the argument of the function $f(x)$.

The five derivatives of $F(t,x)$ used in the first-order approximate boundary conditions can be evaluated exactly and are presented in Ref. 13 along with the following approximate expressions.

$$\begin{aligned} F_x &= f' - \tan\alpha_1 + O(F^3) \\ F_{xx} &= f'' + O(F^3) \\ F_t &= -\alpha_1'(x - x_0)\sec^2\alpha_1 + O(F^3) \\ F_{tx} &= -\alpha_1'\sec^2\alpha_1 + O(F^3) \\ F_{tt} &= -(x - x_0)\sec^2\alpha_1(\alpha_1'' + 2\alpha_1'^2\tan\alpha_1) + O(F^3) \end{aligned} \quad (18)$$

where the $'$ denotes differentiation of $f(x)$ and $\alpha(t)$ with respect to x and t, respectively.

V. Results and Discussions

The method in its reduced steady-state form was tested in Ref. 13 for three NACA airfoils of different thicknesses and at various angles of attack. The results with the approximate boundary conditions on a Cartesian grid agree well with those by the same Euler code (FLO52) with full boundary conditions using body-fitted curvilinear grids for airfoils of thickness ratios up to 15% and anges of attack up to 8 degrees. In this section, we presents results for unsteady flows and coupled fluid-structure simulations for flutter predictions by using the unsteady version of the approximate boundary conditions.

A. Unsteady Flows

The present approximate method is used to calculate the flow over an NACA 0012 airfoil pitching around its quarter-chord point. Experimental data were provided by Landon.[15] The pitching motion of the airfoil is described by the following equation.

$$\alpha(t) = \alpha_m + \alpha_0\sin\omega t \quad (19)$$

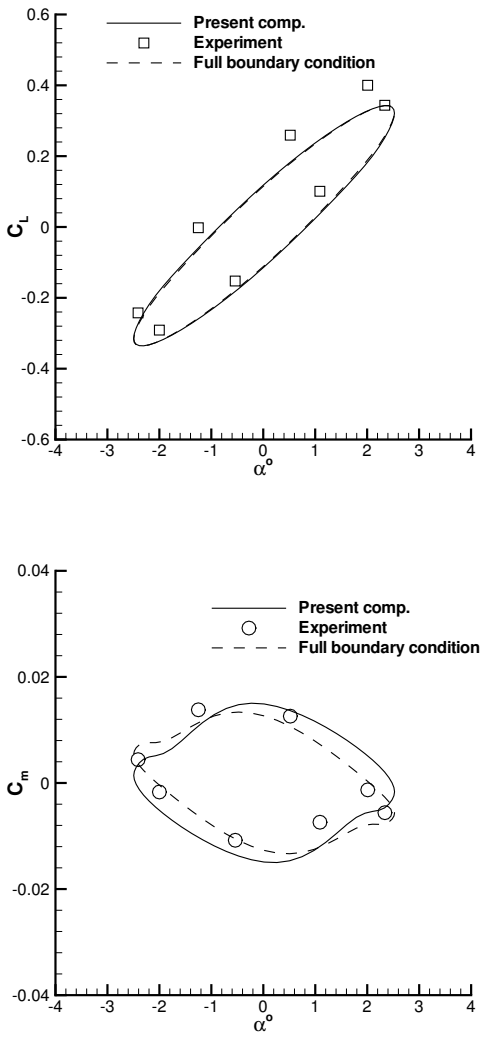

Fig. 1 Comparison of lift and moment coefficients by the present computation with approximate boundary conditions, Euler solution on body-fitted grid with full boundary conditions, and experiment, NACA 0012, $M_\infty = 0.755$, $\alpha_m = 0.016$ deg, $\alpha_0 = 2.51$ deg, $\kappa = 0.0814$.

where ω, α_m and α_0 are constants. The angular frequency ω is related to the reduced frequency defined as

$$\kappa = \frac{\omega c}{2U_\infty} \quad (20)$$

The rectilinear grids used in the unsteady-flow calculations are the same as that used in the above steady-flow computations. The criterion for the convergence of the pseudo-time computations is that the maximum magnitude of the residuals be reduced by more than four orders of magnitude. To satisfy this criterion, the number of the pseudo-time steps is usually 150. The

calculations start from the uniform flow of velocity U_∞ as an initial solution. After three real-time cycles of the airfoil motion an essentially periodic solution is obtained. In this paper six cycles of motion are used to ensure the computed results to be periodic.

The present approximate method is validated by comparing with results obtained by the Euler option of the code NS83 in Ref. 11, 12, on which the present approximate method is based upon. Results are also compared with experimental data. The AGARD CT case 5 of Reference 15 is studied. The airfoil is an NACA 0012 pitching at the free stream Mach number $M_\infty = 0.755, \alpha_m = 0.016\,\text{deg}, \alpha_0 = 2.51\,\text{deg}, \kappa = 0.0814$. The experimental $Re = 5.5 \times 10^6$. The comparisons of the present inviscid computations and the experimental data of the instantaneous lift and moment coefficients vs. the instantaneous angle of attack are presented in Figure 1. The computed instantaneous pressure distributions at the eight phase angles during the sixth cycle of motion are compared with the experimental data in Figure 2. The eight phase angles are 25.3, 67.8, 127.4, 168.4, 210.3, 255.1, 306.6, and 347.2 degrees. The time variation of the computed and experimental data of the surface pressure distributions can be expressed in terms of their Fourier components. Figure 3 shows the comparison of the real and imaginary parts of the first three Fourier modes of the unsteady pressure coefficient over the airfoil surface. The solutions with the full boundary conditions in general give better resolution of the pressure distribution in the high suction areas and better shock positions than the solutions with the approximate boundary conditions compared to the experimental data. The solutions with the approximate boundary conditions show a slight bump when there is a large suction near the leading edge. This is seen in both Figure 2 and the first Fourier mode of the unsteady pressure coefficient shown in Figure 3. However, the overall agreement with both the solutions by the full boundary conditions and the experimental data are good. Batina[16] computed the Euler solutions with full boundary conditions on an unstructured body-fitted grid and compared his solutions with the same experimental data as we have done here. His computed results have qualitatively the same degree of agreement with the experimental data as do the computed results by the present approximate method.

B. Flutter Calculations

We use the current unsteady Euler solver in a coupled CFD-CSD method[4] for the two-dimensional Isogai wing model,[17,18] Case A ($\mu = 60$). This model simulates the bending and torsional motion of a wing cross-section in the outboard portion of a swept wing. It consists of two degrees of freedom, plunging and pitching, for a NACA 64A010 airfoil. We compute this case with the current Euler equations and compare the results in Ref. 4. The details of the structural model can be found in Reference 19 as well as in Refs. 17 and 18.

Figures 4-6 show the flutter computational results for the Isogai wing model at a flight Mach number of 0.825. Plotted in the figures are the time history of the pitching and plunging amplitude computed by the integrated CFD-CSD code with the current Euler solver. Figure 4 is a case with a low speed index $V_f = 0.530$. V_f is defined as

$$V_f = \frac{U_\infty}{b\omega\sqrt{\mu}}$$

where ω is the eigen frequency of the structure. For this low V_f, figure 4 shows that both the pitching and plunging amplitude decays with time, indicating that the aeroelastic system is stable for this particular condition. At a higher V_f, the system may become less and less stable until one or both of the pitching and plunging motions diverge as shown in Figure 5 when $V_f = 0.82$. In between these two V_f conditions, there is a particular point where the system is neutrally stable. This is shown in Figure 6 when $V_f = 0.71$.

A converging point and a diverging point like the above are first identified, from which we can interpolate the V_f in between to obtain an estimate of the neutral point. We then perform a computation with the new V_f to see if it is above or below the stability limit, or perhaps right at the neutral point. It may take several runs for a given freestream Mach number before the V_f corresponding to the neutral stability point can be accurately located by this 'bisection' method. With this method computations for a number of free-stream Mach numbers for the Isogai wing model are performed. The flutter boundary predicted by the present method on a cartesian grid with the first order approximate method is compared in Figure 7 with thosed predicted by Liu et al.[4] and Alonso and Jameson[19] with the full boundary conditions. The agreement is good except for the point at $M_\infty = 0.9$, Many more runs are performed with the present approxmate method to map out the details of the flutter boundary in the transonic range where the flutter boundary may curve back into the unstable region. For example, at $M_\infty = 0.885$, the system initally crosses the stability boundary at $V_f = 0.65$ to become unstable as V_f increases. As V_f increases above 1.83, however, the system becomes stable again until V_f reaches above 3.20 when it returns to being unstable.

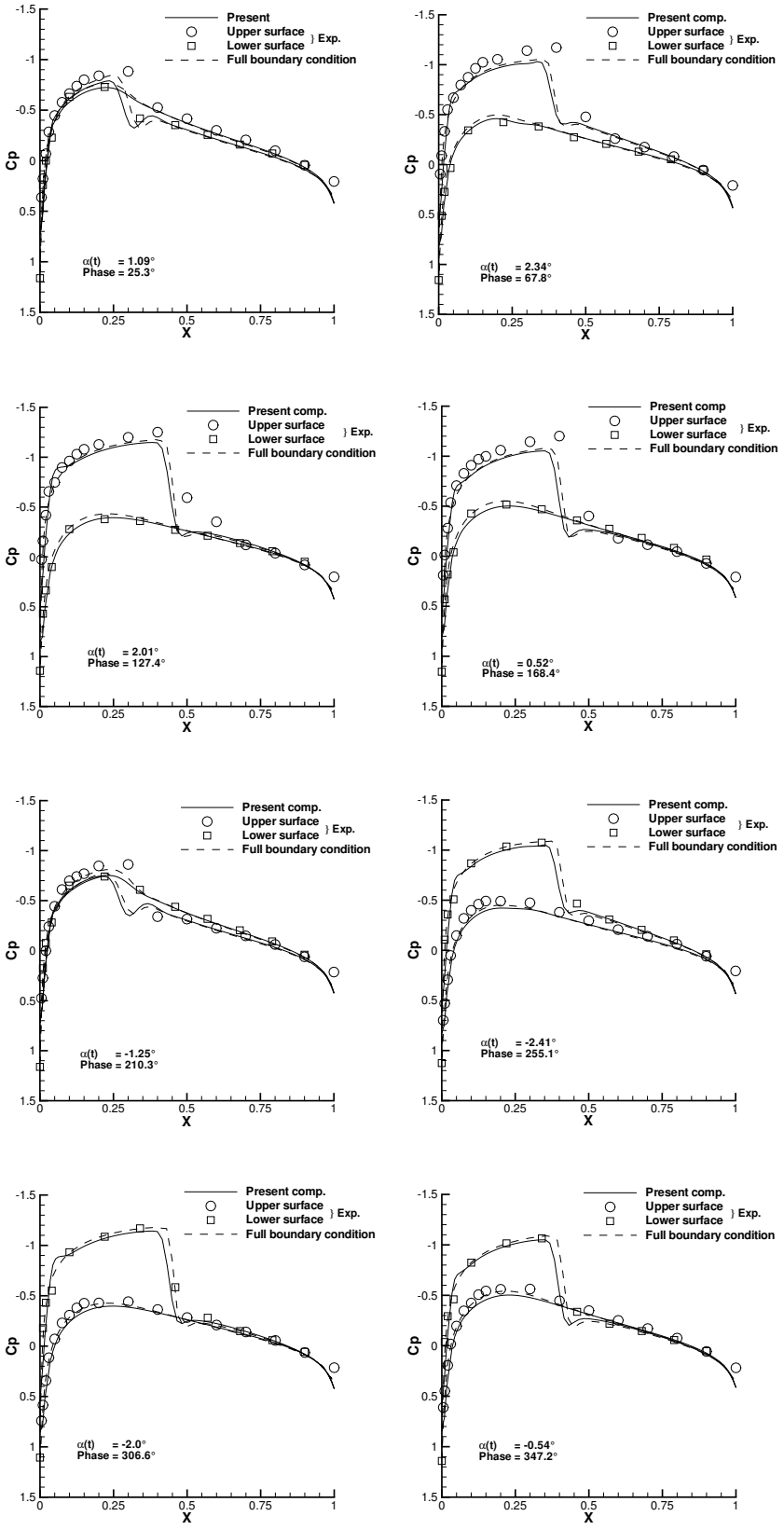

Fig. 2 Comparison of surface pressure distributions by the present computation with approximate boundary conditions, Euler solution on body-fitted grid with full boundary conditions, and experiment, NACA 0012, $M_\infty = 0.755$, $\alpha_m = 0.016\,\mathrm{deg}$, $\alpha_0 = 2.51\,\mathrm{deg}$, $\kappa = 0.0814$.

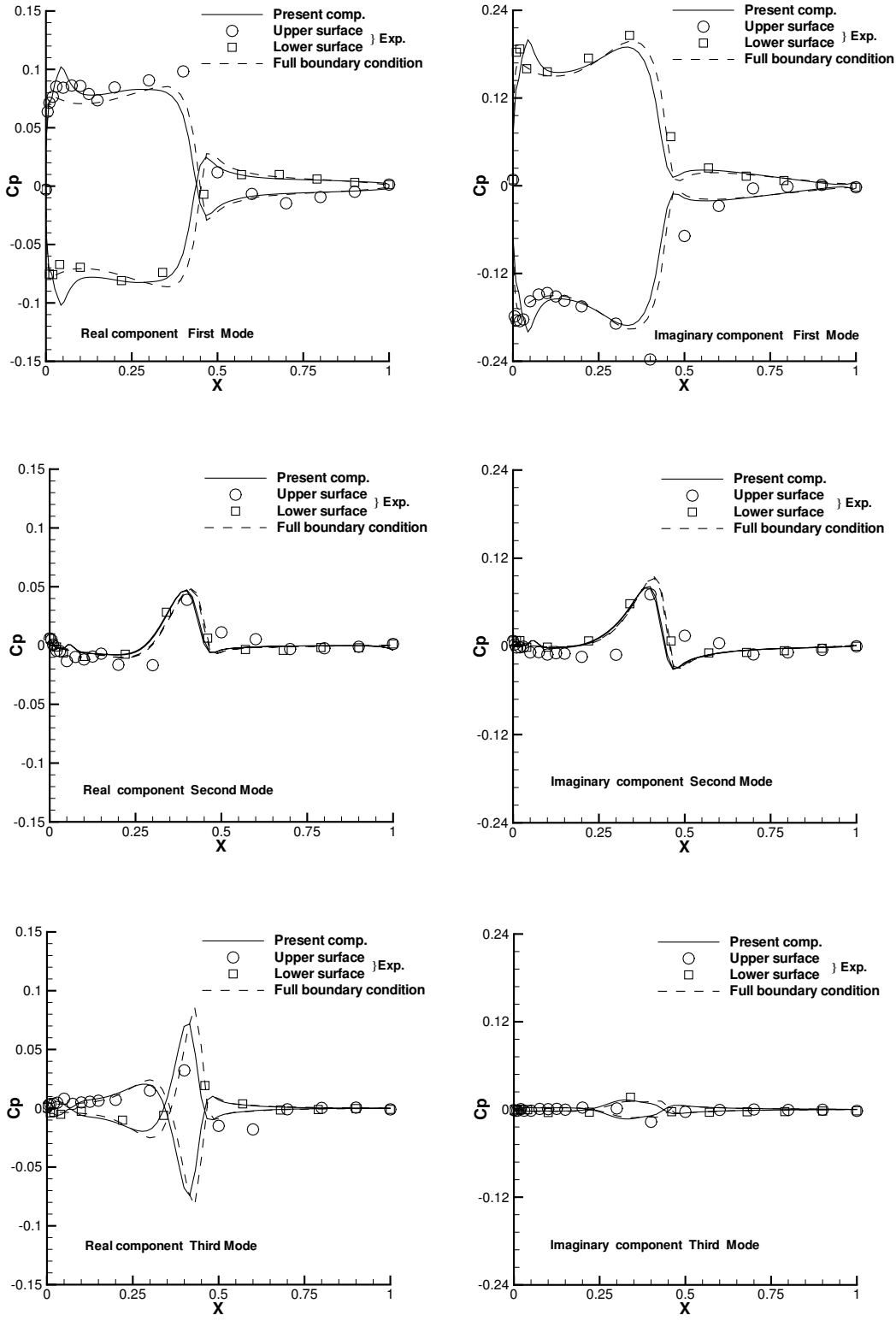

Fig. 3 Comparison of Fourier Components of surface pressure variations by the present computation with approximate boundary conditions, Euler solution on body-fitted grid with full boundary conditions, and experiment, NACA 0012, $M_\infty = 0.755$, $\alpha_m = 0.016\,\mathrm{deg}$, $\alpha_0 = 2.51\,\mathrm{deg}$, $\kappa = 0.0814$.

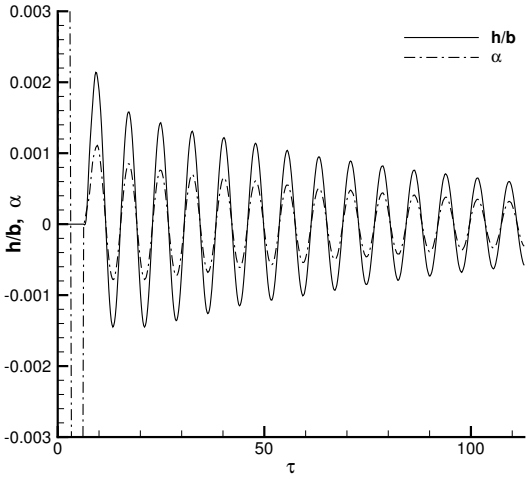

Fig. 4 Time history of pitching and plunging motion for the Isogai wing model for $M_\infty = 0.825$, and $V_f = 0.530$, stable situation.

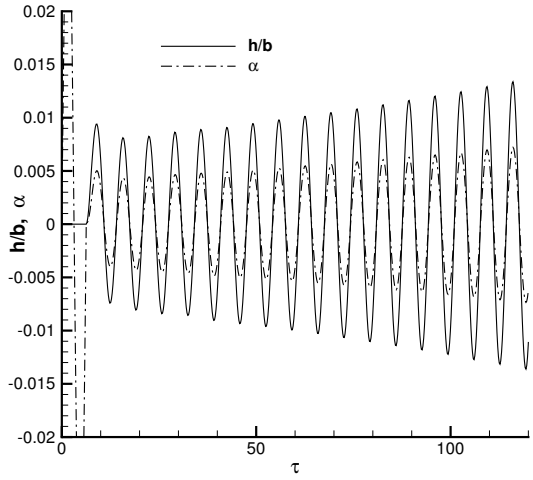

Fig. 5 Time history of pitching and plunging motion for the Isogai wing model for $M_\infty = 0.825$, and $V_f = 0.78$, unstable situation.

Despite the use of the first order approximate boundary conditions, the code is also able to simulate LCO. Figure 8 shows such a case at $M_\infty = 0.825$ and $V_f = 1.45$. For each flight Mach number, the code predicts LCO when V_f is sufficiently large after it crosses the flutter boundary. The circles shown in Figure 7 mark such conditions predicted by the present computations. It is, however, not clear if such predictions are reliable since the computations are based on an inviscid model and also with the approximate boundary conditions. An interactive boundary-layer method like the one used in CAP-TSD may be used to improved the accuracy of the model.

VI. Conclusions

This paper presents an efficient numerical method for solving the unsteady Euler equations on stationary Cartesian grids. It is shown that the boundary conditions on the surface of an airfoil can be approximated by their first-order expressions on the mean position of the airfoil chord while the full Euler equations are solved in the flow field on stationary non-body-conforming Cartesian type of grids. For unsteady flows, the calculated instantaneous lift, moment, surface pressure distributions and the Fourier components of the surface pressure variations by the approximate method agree well with the experimental data for the NACA0012 airfoil with oscillating pitch angles up to 3 degrees at transonic speeds. There is no restriction on the size of the mean angle of attack.

The unsteady flow solver is used in a coupled CFD-CSD simulation for airfoil flutter. The resulting code can be used to predict flutter efficiently. The com-

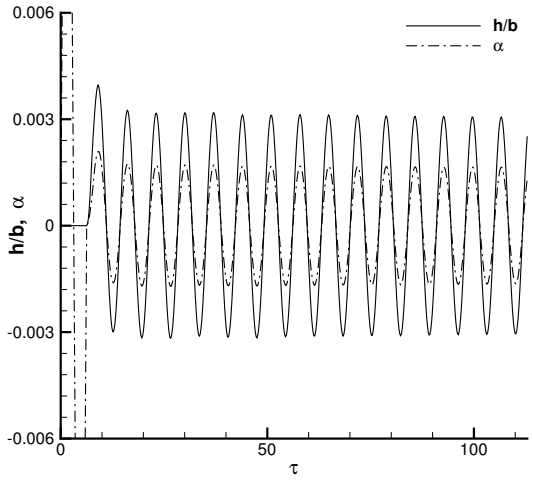

Fig. 6 Time history of pitching and plunging motion for the Isogai wing model for $M_\infty = 0.825$, and $V_f = 0.71$, neutral situation.

puted flutter boundary by the present method on a cartesian grid with approximate boundary conditions are in good agreement with results by Euler solvers on body-fitted grids with full boundary conditions for the Isogai wing model except near supersonic speeds. The method is also found to simulate LCO solutions although the LCO amplitude may not be reliable with the assumed approximate boundary conditions. The advantage of using a single stationary non-body-conforming rectilinear grid opens the door for the efficient computation of unsteady fluid-structure inter-

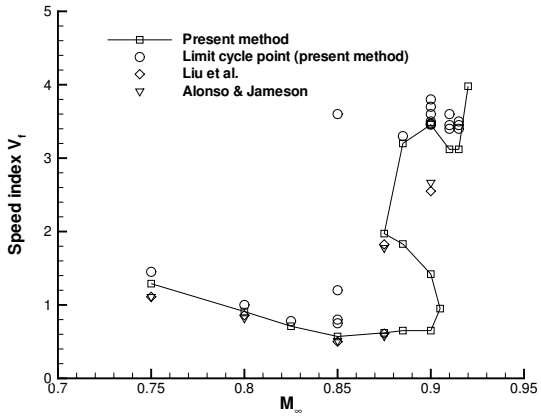

Fig. 7 Computed flutter boundary for the Isogai wing model.

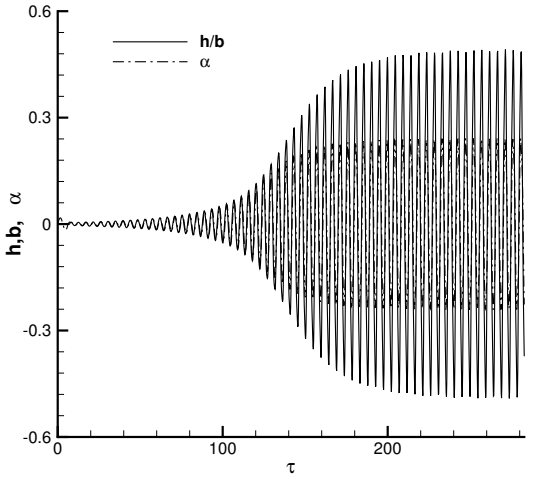

Fig. 8 Time history of pitching and plunging motion for the Isogai wing model for $M_\infty = 0.825$, and $V_f = 1.45$

action problems involving small unsteadily deforming airfoils or wings of small thickness by using the present approximate boundary condition method.

Acknowledgement

This work is supported by NASA Langley Research Center, contract number NAG-1-02050.

References

[1]Rodden, W. P. and Johnson, E. H., *MSC/NASTRAN Aeroelastic Analysis User's Guide, Version 68*, The Macneal-Schwender Corporation, Los Angeles, 1994.

[2]Lee-Rausch, E. M. and Batina, J. T., "Wing Flutter Boundary Prediction Using Unsteady Euler Aerodynamic Method," *Journal of Aircraft*, Vol. 32, No. 2, Mar.-Apr. 1995, pp. 416–422.

[3]Lee-Rausch, E. M. and Batina, J. T., "Wing Flutter Computations Using an Aerodynamic Model Based on the Navier-Stokes Equations," *Journal of Aircraft*, Vol. 33, No. 6, Nov.-Dec. 1996, pp. 1139–1147.

[4]Liu, F., Cai, J., Zhu, Y., Wong, A. S. F., and Tsai, H.-M., "Calculation of Wing Flutter by a Coupled Fluid-Structure Method," *Journal of Aircraft*, Vol. 38, No. 2, Mar.-Apr. 2001, pp. 334–342.

[5]Gibbons, M., "Aeroelastice Calculations Using CFD for a Typical Business Jet Model," NASA CR 4753, 1996.

[6]Bartels, R., "Flow and Turbulence Modeling and Computation of Shock Buffet Onset for Conventional and Supercritical Airfoils," NASA TP 1998-206908, 1998.

[7]Tang, L., Bartels, R., Chen, P., and Liu, D. D., "Numerical Investigation of Transonic Limit Oscillations of a 2-D supercritical Wing," AIAA Paper 2001-1290, 2001.

[8]Batina, J. T., "A Finite-Difference Approximate-Factorization Algorithm for Solution of the Unsteady Transonic Small-Disturbance Equation," NASA TP 3129, Jan. 1992.

[9]Edwards, J., "Transonic Shock Oscillations Calculated with a New Interactive Boundary Layer Coupling Method," AIAA Paper 93-0777, 1993.

[10]Edwards, J., "Transonic Shock Oscillations and Wing Flutter Calculated with an Interactive Boundary Layer Coupling Method," Euromech-colloquium 349, simulation of fluid-structure interaction in aeronautics, gottingen, germany, Sept. 1996.

[11]Jameson, A., "Time dependent calculations using multigrid, with applications to unsteady flows past airfoils and wings," AIAA Paper 91–1596, June 1991, 10th AIAA Computational Fluid Dynamics Conference.

[12]Liu, F. and Ji, S., "Unsteady Flow Calculations with a Multigrid Navier-Stokes Method," *AIAA Journal*, Vol. 34, No. 10, Oct. 1996, pp. 2047–2053.

[13]Gao, C., Luo, S., and Liu, F., "Calculation of Unsteady Transonic Flow by an Euler Method with Small Perturbation Boundary Conditions," AIAA Paper 2003-1267, Jan. 2003.

[14]Jameson, A., Schmidt, W., and Turkel, E., "Numerical Solutions of the Euler Equations by Finite Volume Methods Using Runge-Kutta Time-Stepping Schemes," AIAA Paper 81–1259, June 1981.

[15]Landon, R. H., "NACA 0012 Oscillating and Transient Pitching, Compendium of Unsteady Aerodynamic Measurements, Data Set 3," AGARD Report R-702, Aug. 1982.

[16]Batina, J. T., "Unsteady Euler Airfoil Solutions Using Unstructured Dynamic Meshes," *AIAA Journal*, Vol. 28, No. 8, Aug. 1990, pp. 1381–1388.

[17]Isogai, K., "On the Transonic-Dip Mechanism of flutter of a Sweptback Wing," *AIAA Journal*, Vol. 17, No. 7, 1979, pp. 793–795.

[18]Isogai, K., "On the Transonic-Dip Mechanism of flutter of a Sweptback Wing: Part II," *AIAA Journal*, Vol. 19, No. 7, 1981, pp. 1240–1242.

[19]Alonso, J. J. and Jameson, A., "Fully-Implicit Time-Marching Aeroelastic Solutions," AIAA Paper 94–0056, Jan. 1994.